NATIONAL ADVISORY COMMITTEE FOR AERONAUTICS

TECHNICAL NOTE 2741

INVESTIGATION OF THE INFLUENCE OF FUSELAGE AND TAIL SURFACES ON LOW-SPEED STATIC STABILITY AND ROLLING CHARACTERISTICS OF A SWEPT-WING MODEL

By John D. Bird, Jacob H. Lichtenstein,
and Byron M. Jaquet

Langley Aeronautical Laboratory
Langley Field, Va.

Washington
July 1952

1Z

NATIONAL ADVISORY COMMITTEE FOR AERONAUTICS

TECHNICAL NOTE 2741

INVESTIGATION OF THE INFLUENCE OF FUSELAGE AND TAIL SURFACES ON LOW-SPEED STATIC STABILITY AND ROLLING CHARACTERISTICS OF A SWEPT-WING MODEL[1]

By John D. Bird, Jacob H. Lichtenstein, and Byron M. Jaquet

SUMMARY

A wind-tunnel investigation was made in the Langley stability tunnel to determine the influence of the fuselage and tail surfaces on the static stability and rotary derivatives in roll of a transonic airplane configuration which had 45° sweptback wing and tail surfaces.

The tests made in straight flow showed that the wing alone has marginal longitudinal stability characteristics near maximum lift. The variation of rolling-moment coefficient with angle of yaw of the complete model is almost the same as for the wing alone.

The results of the tests made in simulated rolling flight indicate that for this model the effects of the fuselage and tail surfaces on the rate of change of the rolling-moment, yawing-moment, and lateral-force coefficients with wing-tip helix angle are small in comparison with the effect of the angle of attack on these rotary characteristics. The vertical tail produces larger increments of the rate of change of lateral-force and yawing-moment coefficients with wing-tip helix angle than the fuselage or horizontal tail.

INTRODUCTION

Estimation of the dynamic flight characteristics of aircraft requires a knowledge of the component forces and moments arising from the orientation

[1]Supersedes the recently declassified NACA RM L7H15, "Investigation of the Influence of Fuselage and Tail Surfaces on Low-Speed Static Stability and Rolling Characteristics of a Swept-Wing Model" by John D. Bird, Jacob H. Lichtenstein, and Byron M. Jaquet, 1947.

of the model with respect to the air stream (static derivatives) and from the rate of angular displacement with respect to the air stream (rotary derivatives). The forces and moments arising from orientation of the model are determined by use of conventional wind-tunnel tests, and, until the recent use of large amounts of wing sweep, the rotary derivatives at other than very high angles of attack were satisfactorily estimated by theoretical means. Unpublished data and the calculations of reference 1, however, show that for swept wings the derivatives in roll cannot be satisfactorily predicted by existing theoretical means, particularly at moderate and high lift coefficients. An investigation therefore was conducted to determine the influence of the tail surfaces and fuselage of an airplane on the low-speed rotary derivatives in roll of a transonic airplane configuration having 45° sweptback wing and tail surfaces. The static stability characteristics of various configurations of the model were determined in the course of the tests. The results of this investigation are reported herein.

SYMBOLS

The results of the tests are presented as standard coefficients of forces and moments which are referred to the stability axes the origin of which is assumed to be at the projection on the plane of symmetry of the quarter-chord point of the mean geometric chord of the wing of the model tested. The stability axes system is shown in figure 1. The coefficients and symbols used herein are defined as follows:

C_L lift coefficient $\left(\frac{L}{qS}\right)$

C_D drag coefficient $\left(\frac{D}{qS}\right)$

C_Y lateral-force coefficient $\left(\frac{Y}{qS}\right)$

C_l rolling-moment coefficient $\left(\frac{L'}{qSb}\right)$

C_m pitching-moment coefficient $\left(\frac{M}{qSc}\right)$

C_n yawing-moment coefficient $\left(\frac{N}{qSb}\right)$

L	lift, negative of Z-force in figure 1
D	drag
Y	lateral force
L'	rolling moment about X-axis
M	pitching moment about Y-axis
N	yawing moment about Z-axis
q	dynamic pressure $\left(\frac{1}{2}\rho V^2\right)$
ρ	mass density of air
V	free-stream velocity
S	wing area
b	span of wing
c	chord of wing, measured parallel to axis of symmetry
α	angle of attack, measured in plane of symmetry, degrees
ψ	angle of yaw, degrees
$\frac{pb}{2V}$	wing-tip helix angle, radians
p	rate of roll, radians per second

$$C_{Y_\psi} = \frac{\partial C_Y}{\partial \psi}$$

$$C_{n_\psi} = \frac{\partial C_n}{\partial \psi}$$

$$C_{l_\psi} = \frac{\partial C_l}{\partial \psi}$$

$$C_{Y_p} = \frac{\partial C_Y}{\partial \frac{pb}{2V}}$$

$$C_{n_p} = \frac{\partial C_n}{\partial \frac{pb}{2V}}$$

$$C_{l_p} = \frac{\partial C_l}{\partial \frac{pb}{2V}}$$

APPARATUS AND TESTS

The tests described herein were conducted in the 6-foot-diameter rolling-flow test section of the Langley stability tunnel. This section is equipped with a motor-driven rotor which imparts a twist to the air stream so that a model mounted rigidly in the tunnel is in a field of flow similar to that which exists about an airplane in rolling flight (reference 2). The test model is mounted on a single strut which is connected to a conventional six-component balance system.

The model used for the subject tests was a transonic configuration having 45° sweptback wing and tail surfaces. These surfaces had NACA 0012 airfoil sections normal to the leading edge (thickness ratio 0.085 parallel to plane of symmetry) and a taper ratio of 1. The fuselage was a body of revolution which had a circular-arc profile and a fineness ratio of 8.34. A view of the model mounted in the tunnel is shown as figure 2, and the geometric characteristics of the model are given in figure 3.

The test configurations and the symbols used in identifying the data in the figures are given in the following table. The wing-alone data were obtained from reference 3.

Wing	W
Fuselage	F
Wing and fuselage	W + F
Wing, fuselage, and vertical tail	W + F + V
Wing, fuselage, vertical tail, and horizontal tail	W + F + V + H

Six-component measurements were made in straight flow through the angle-of-attack range from $\alpha = 0^\circ$ to $\alpha = 26^\circ$ at values of ψ of 0° and $\pm 5^\circ$ and through the yaw range from $\psi = 0^\circ$ to $\psi = 30^\circ$ at values of α of 0°, 6.2°, and 12.5°. These same measurements at $\psi = 0^\circ$ were made in rolling flow at positive and negative rolling velocities corresponding to values of $\frac{pb}{2V}$ of ± 0.0446. Rotation in positive and negative

directions was used in order to eliminate any asymmetrical effects associated with the model or air stream. All tests were run at a dynamic pressure of 40 pounds per square foot which corresponds to a Mach number of 0.17 and a Reynolds number of 1,400,000.

CORRECTIONS

The following corrections for jet-boundary effects were applied to the data:

$$\Delta C_D = \delta_w \left(\frac{S}{C}\right) C_{L_T}{}^2$$

$$\Delta C_l = K C_{l_T}$$

$$\Delta \alpha = 57.3 \delta_w \left(\frac{S}{C}\right) C_{L_T}$$

where

Δ	jet-boundary correction
δ_w	boundary-correction factor from reference 4
S	wing area, square feet
C	tunnel cross-sectional area, square feet
C_{L_T}	uncorrected lift coefficient
C_{l_T}	uncorrected rolling-moment coefficient
K	correction factor from reference 5 corrected for application to these tests by taking into account changes in model and tunnel size

No corrections were made for tunnel blocking or support-strut tares. Tares were determined for a few cases and the results indicated that, although there were large tare corrections to the drag coefficient, the corrections to the derivatives of the forces and moments with respect to yaw angle and wing-tip helix angle were in most cases negligible.

Although reference 6 presents a more exact method of determining δ_w, the method used herein, as outlined in reference 4, is believed to give sufficiently accurate results for the model and tunnel used in this investigation.

RESULTS AND DISCUSSION

Presentation of Data

The results of this investigation are presented in figures 4 to 9. Curves are given in each plot for all configurations tested in order to facilitate comparison. Figure 4 presents the lift, drag, and pitching-moment characteristics of the test configurations for the angle-of-attack range at $\psi = 0^\circ$, together with a cross plot of the pitching-moment coefficient against lift coefficient. Figures 5, 6, and 7 present the variation of the rolling-moment, yawing-moment, and lateral-force coefficients with angle of yaw for angles of attack of 0°, 6.2°, and 12.5°. The derivatives C_{l_ψ}, C_{n_ψ}, and C_{Y_ψ} are presented for the angle-of-attack range in figure 8. Figure 9 presents the derivatives C_{l_p}, C_{n_p}, and C_{Y_p} for the angle-of-attack range.

Characteristics in Straight Flow

The longitudinal stability characteristics of all model configurations other than the complete model and the fuselage alone were marginal in the critical region near maximum lift. The longitudinal stability characteristics of the complete model are satisfactory for the entire lift range (fig. 4). Marginal characteristics for the wing alone are predicted by the correlation of longitudinal stability characteristics of swept wings presented in reference 7.

The curves of figures 5, 6, and 7 indicate approximately a linear variation of yawing-moment, rolling-moment, and pitching-moment coefficients with angle of yaw for angles of attack up to 12.5°.

The curves of figure 8 indicate that, up to maximum lift, C_{l_ψ} is primarily a function of the characteristics of the wing alone. This fact is evidenced by the proximity of the curves of C_{l_ψ} plotted against angle of attack for the various test configurations. With regard to C_{n_ψ}, the vertical tail produces a stabilizing effect which, except at very high angles of attack, is larger than the destabilizing effect (positive increment of C_{n_ψ}) produced by the fuselage (fig. 8). The

influence of the vertical tail and the fuselage on C_{Y_ψ} is of the same sign except at high angles of attack (fig. 8).

Characteristics in Rolling Flow

From calibration tests it was determined that the lift, drag, and pitching-moment coefficients of the model were almost independent of the rate of rotation; whereas the lateral-force, rolling-moment, and yawing-moment coefficients varied linearly with rate of rotation. The derivatives, however, presented herein were obtained from tests made through the angle-of-attack range at values of $\frac{pb}{2V}$ of ± 0.0446.

The rolling moment due to rolling C_{l_p} for the complete model, as has been found for the wing alone, becomes more negative (increased damping) as the angle of attack is increased and remains so to a point below the angle of attack for maximum lift coefficient where a large decrease in damping occurs (fig. 9). The increase of damping in the low angle-of-attack range is attributed to increases in the slopes of the curves of C_L and C_D plotted against angle of attack. The addition of the fuselage to the wing causes a small reduction in the negative value of C_{l_p} at low and moderate angles of attack and a large reduction at high angles of attack, in spite of the fact that the fuselage causes a slight increase in the lift-curve slope. (See fig. 4.) A possible explanation of these results is that a load of the angle-of-attack type probably is carried across the fuselage, but since the fuselage is a body of revolution and air forces must, to a great extent, act normal to the surface, a load due to rolling would not be expected to be carried across the fuselage. The addition of the vertical and horizontal tails generally causes very small increases in C_{l_p}. For almost the entire angle-of-attack range, however, larger values of C_{l_p} were obtained for the wing alone than for the complete model.

The yawing moment due to rolling C_{n_p} for the complete model follows the trend of the wing alone in that the derivative becomes positive at high angles of attack. The positive values reached, however, are not so high as for the wing alone (fig. 9). The most pronounced effect of all the individual configuration changes on the curve of C_{n_p} plotted against angle of attack is the negative increment contributed by the vertical tail (fig. 9). The value of C_{n_p} of the fuselage was small and positive throughout the angle-of-attack range.

The lateral force due to rolling C_{Y_p} varies almost linearly with angle of attack over the low angle-of-attack range for all test

configurations but falls off before maximum lift is reached (fig. 9). As in the case of C_{n_p}, the vertical tail also produces the largest increment of C_{Y_p} of all the components added to the wing. The effects of the fuselage and horizontal tail are small, as would be expected.

In general, the effects of the fuselage and tail surfaces on the values of the derivatives C_{l_p}, C_{n_p}, and C_{Y_p} of the wing are small in comparison with the effects of angle of attack on these derivatives.

CONCLUSIONS

Wind-tunnel tests for determining the static stability characteristics and the rotary derivatives in roll of a transonic model configuration having 45° sweptback wing and tail surfaces indicate the following conclusions:

1. The longitudinal stability characteristics of the wing alone and the model without the horizontal tail surfaces are marginal in the critical region near maximum lift. The characteristics of the complete model are satisfactory.

2. The variation of the lateral-stability parameter C_{l_ψ} is primarily a function of the characteristics of the wing alone up to maximum lift.

3. The addition of the fuselage and horizontal tail surfaces to the wing has little effect on the rate of change of the rolling-moment, yawing-moment, and lateral-force coefficients with wing-tip helix angle.

4. The addition of the vertical tail to the model produces appreciable increments in the rate of change of the rolling-moment, yawing-moment, and lateral-force coefficients with wing-tip helix angle, but these variations are small in comparison with the effects of angle of attack on these rotary characteristics.

Langley Aeronautical Laboratory
National Advisory Committee for Aeronautics
Langley Field, Va., August 21, 1947

REFERENCES

1. Weissinger, J.: The Lift Distribution of Swept-Back Wings. NACA TM 1120, 1947.

2. MacLachlan, Robert, and Letko, William: Correlation of Two Experimental Methods of Determining the Rolling Characteristics of Unswept Wings. NACA TN 1309, 1947.

3. Feigenbaum, David, and Goodman, Alex: Preliminary Investigation at Low Speeds of Swept Wings in Rolling Flow. NACA RM L7E09, 1947.

4. Silverstein, Abe, and White, James A.: Wind-Tunnel Interference with Particular Reference to Off-Center Positions of the Wing and to the Downwash at the Tail. NACA Rep. 547, 1936.

5. Swanson, Robert S.: Jet-Boundary Corrections to a Yawed Model in a Closed Rectangular Wind Tunnel. NACA ARR, Feb. 1943.

6. Eisenstadt, Bertram J.: Boundary-Induced Upwash for Yawed and Swept-Back Wings in Closed Circular Wind Tunnels. NACA TN 1265, 1947.

7. Shortal, Joseph A., and Maggin, Bernard: Effect of Sweepback and Aspect Ratio on Longitudinal Stability Characteristics of Wings at Low Speeds. NACA TN 1093, 1946.

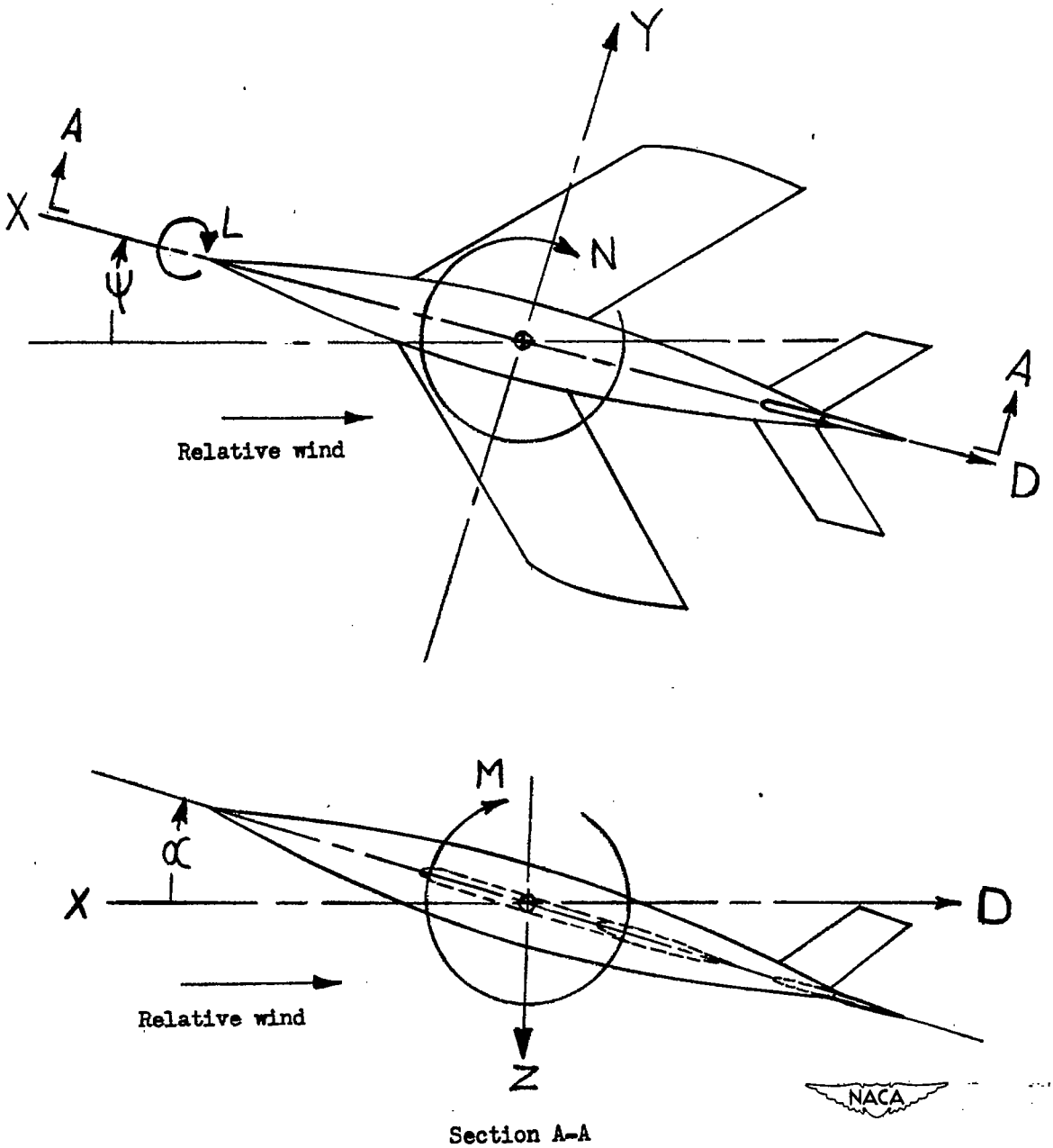

Figure 1.- Stability system of axes. Positive values of forces, moments, and angles are indicated by arrows.

Figure 2.- Complete model in tunnel.

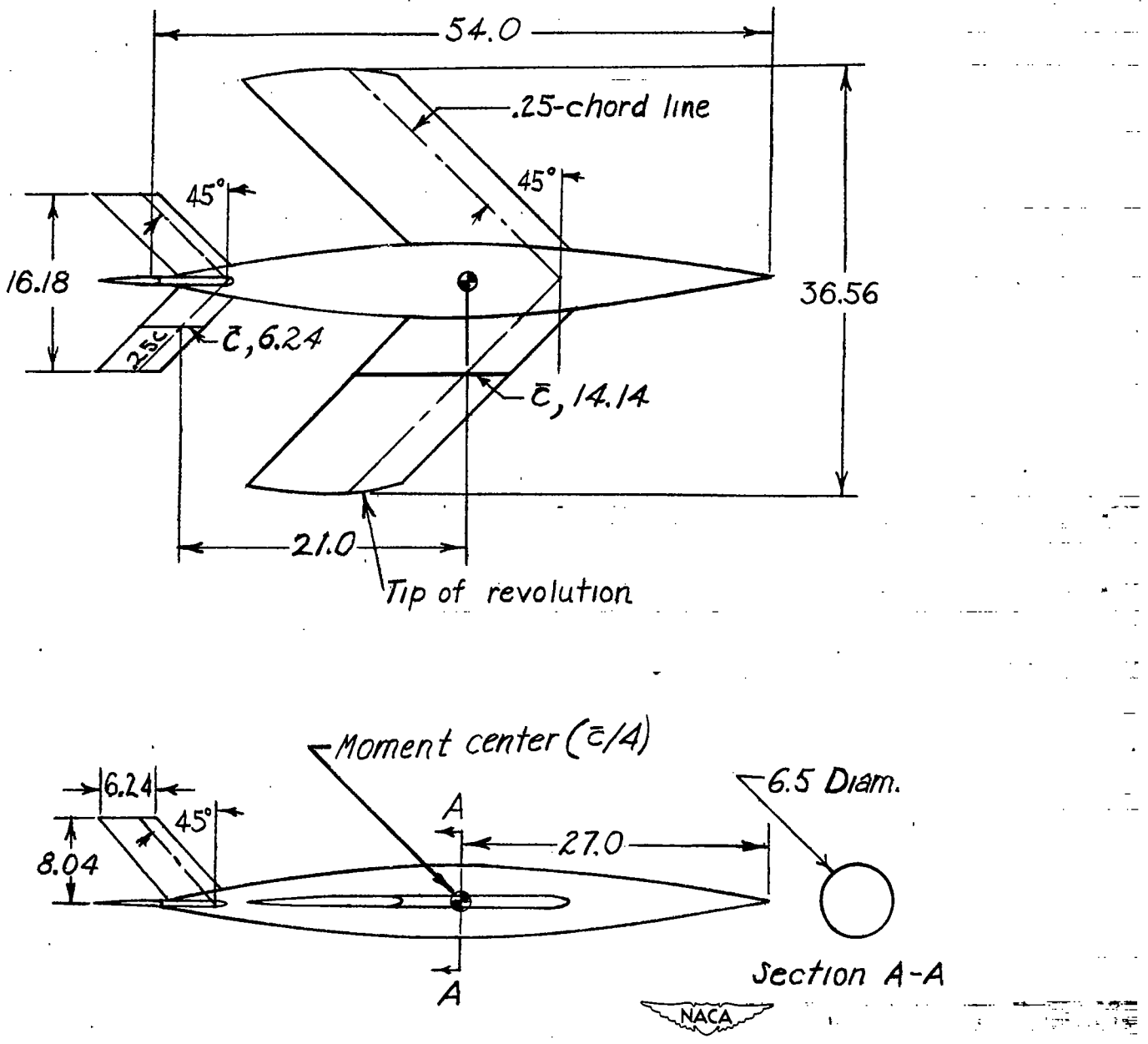

Figure 3.- Geometric characteristics of model. Wing aspect ratio, 2.61. All dimensions in inches.

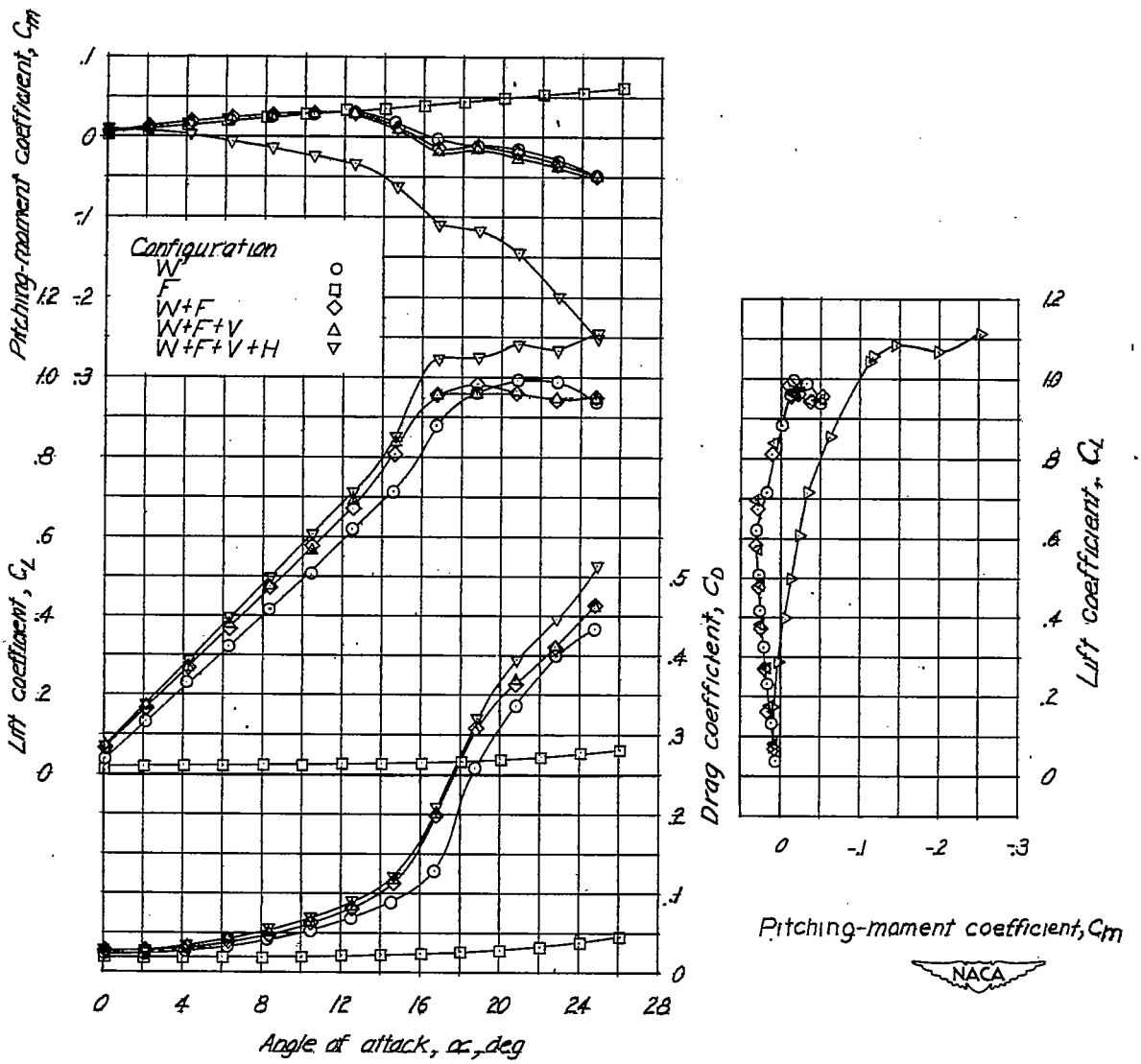

Figure 4.- Variation of lift, drag, and pitching-moment coefficients with angle of attack for all model configurations. $\psi = 0^\circ$.

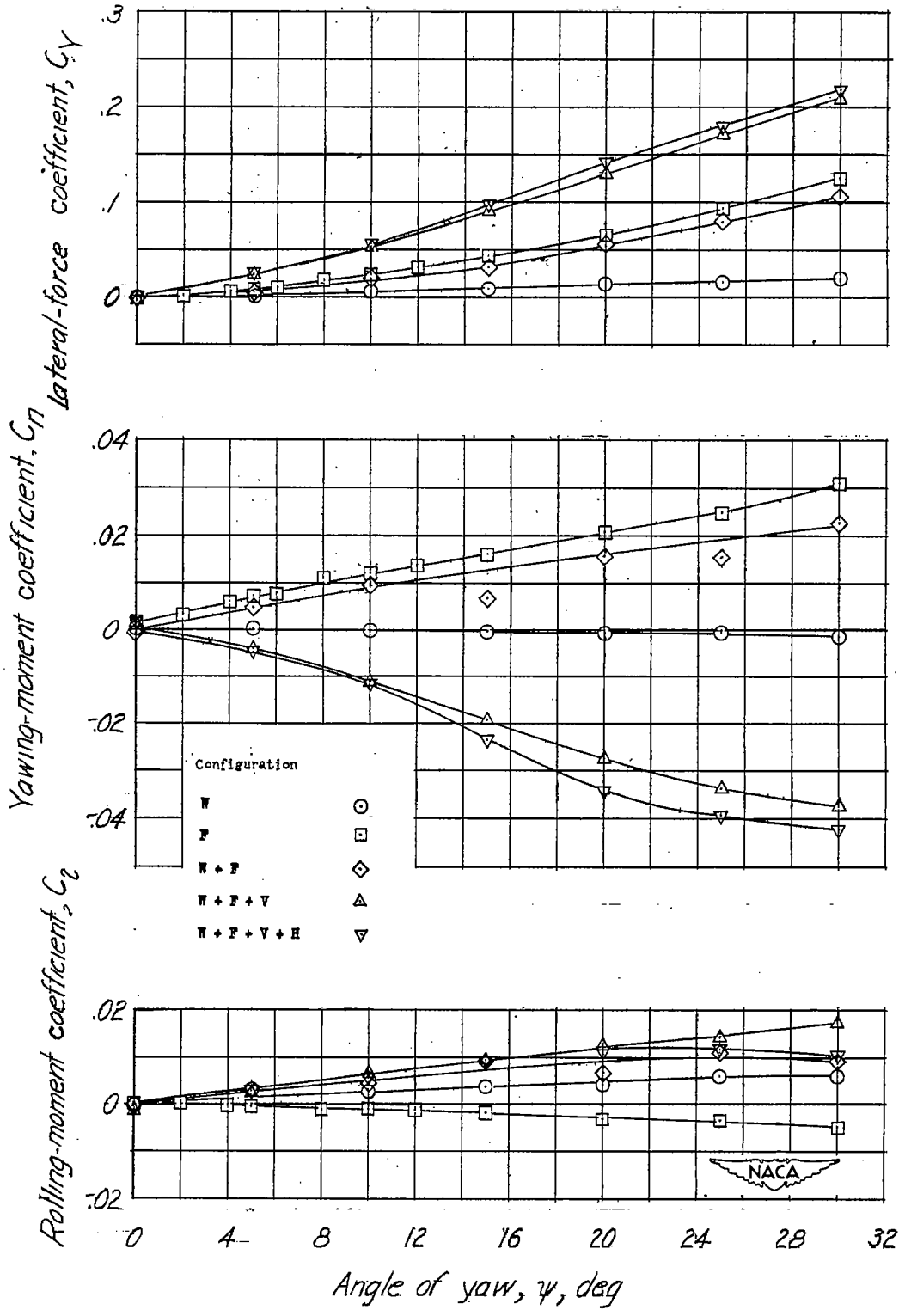

Figure 5.- Variation of rolling-moment, yawing-moment, and lateral-force coefficients with angle of yaw for all model configurations. $\alpha = 0^\circ$.

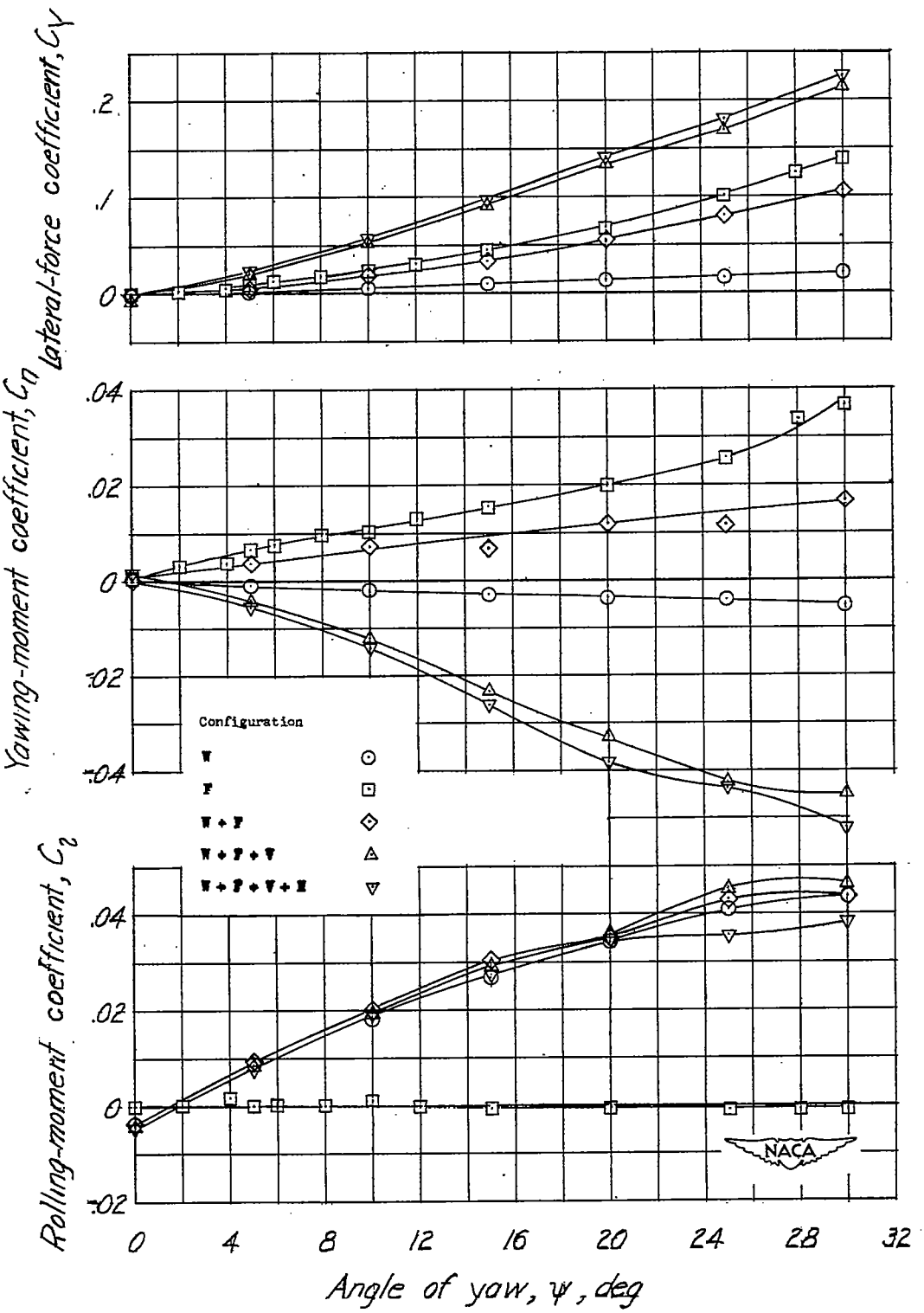

Figure 6.- Variation of rolling-moment, yawing-moment, and lateral-force coefficients with angle of yaw for all model configurations. $\alpha = 6.2^\circ$.

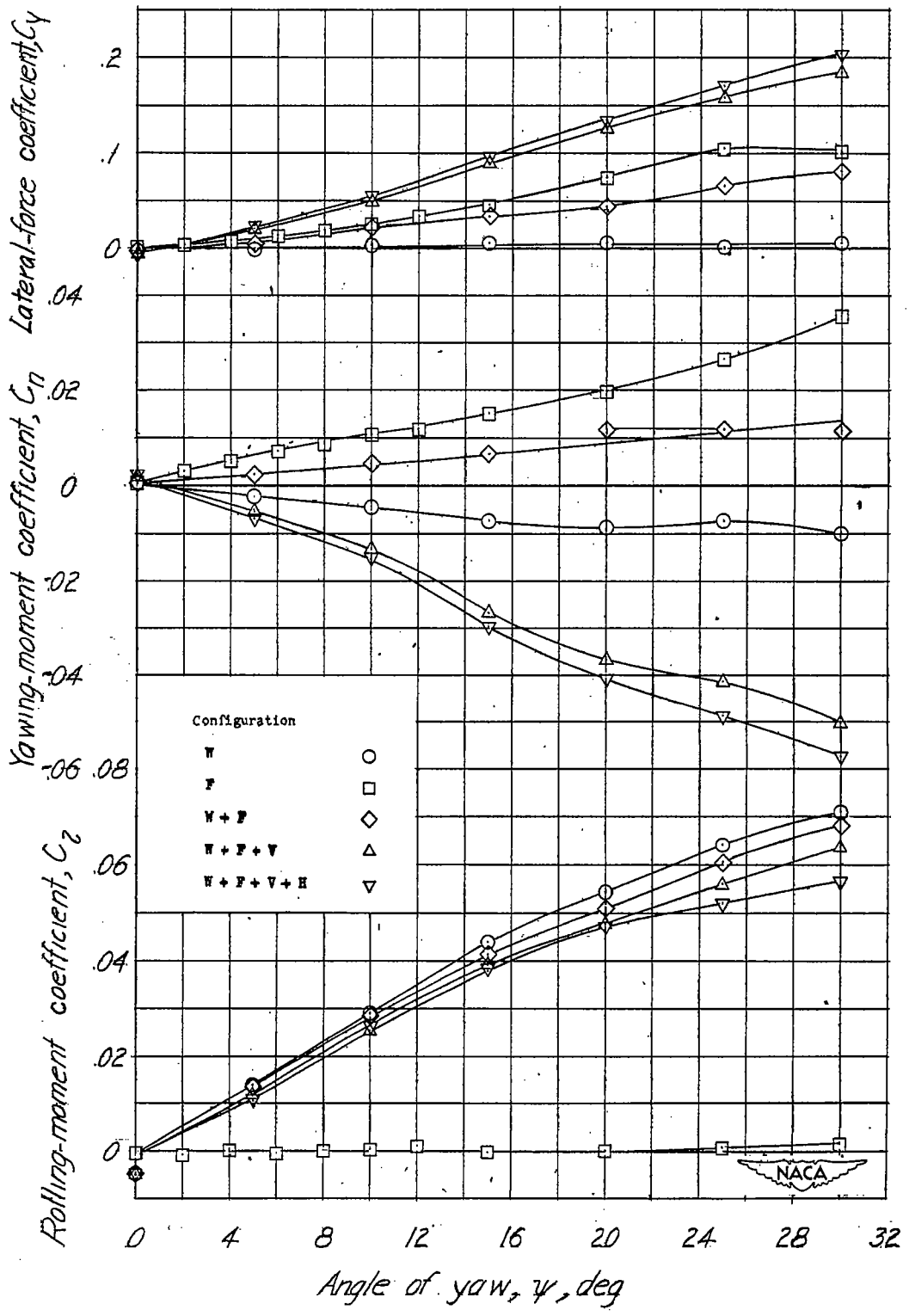

Figure 7.- Variation of rolling-moment, yawing-moment, and lateral-force coefficients with angle of yaw for all model configurations. $\alpha = 12.5^\circ$.

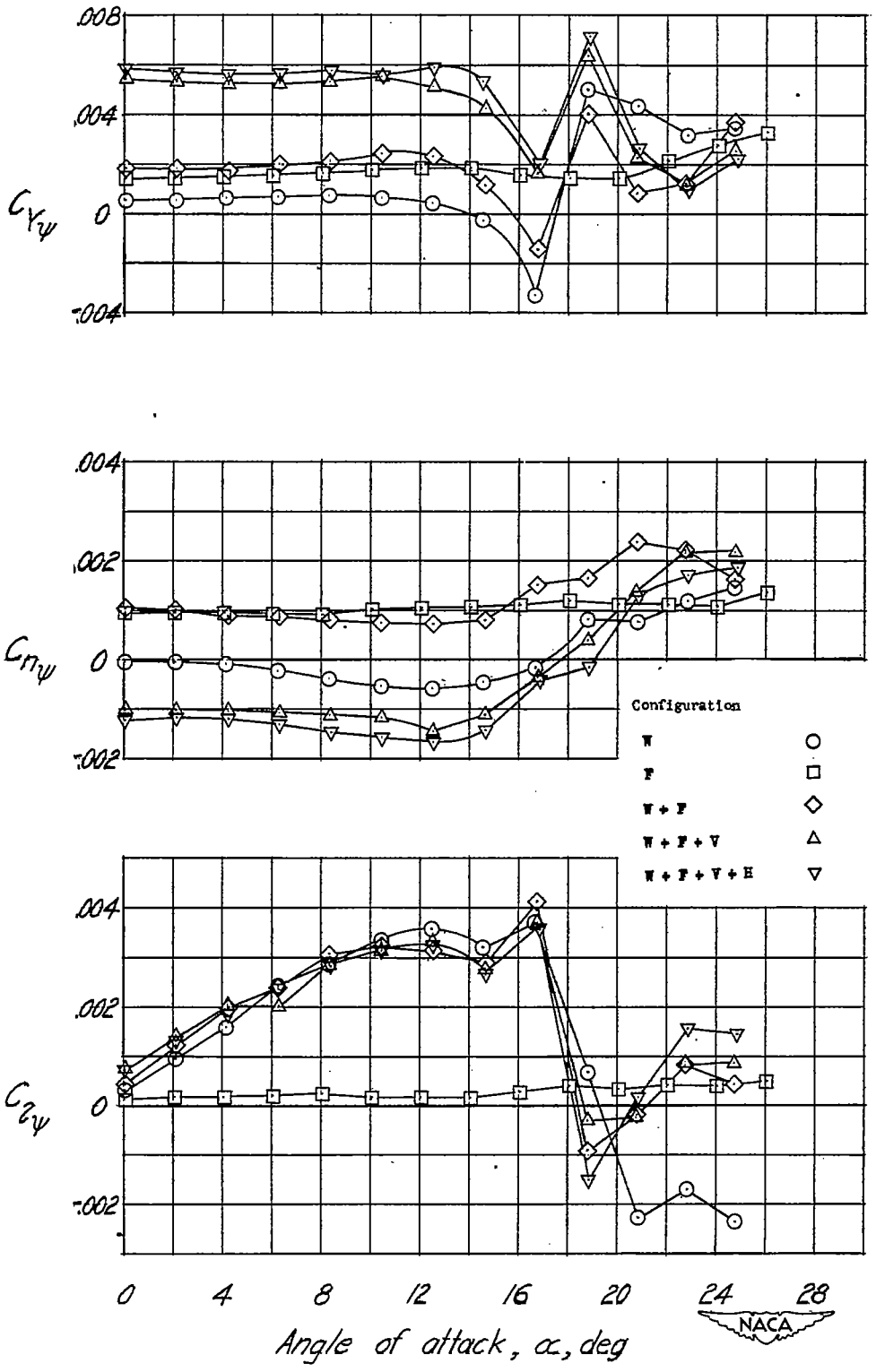

Figure 8.- Variation of C_{l_ψ}, C_{n_ψ}, and C_{Y_ψ} with angle of attack for all model configurations. $\psi = 0^\circ$.

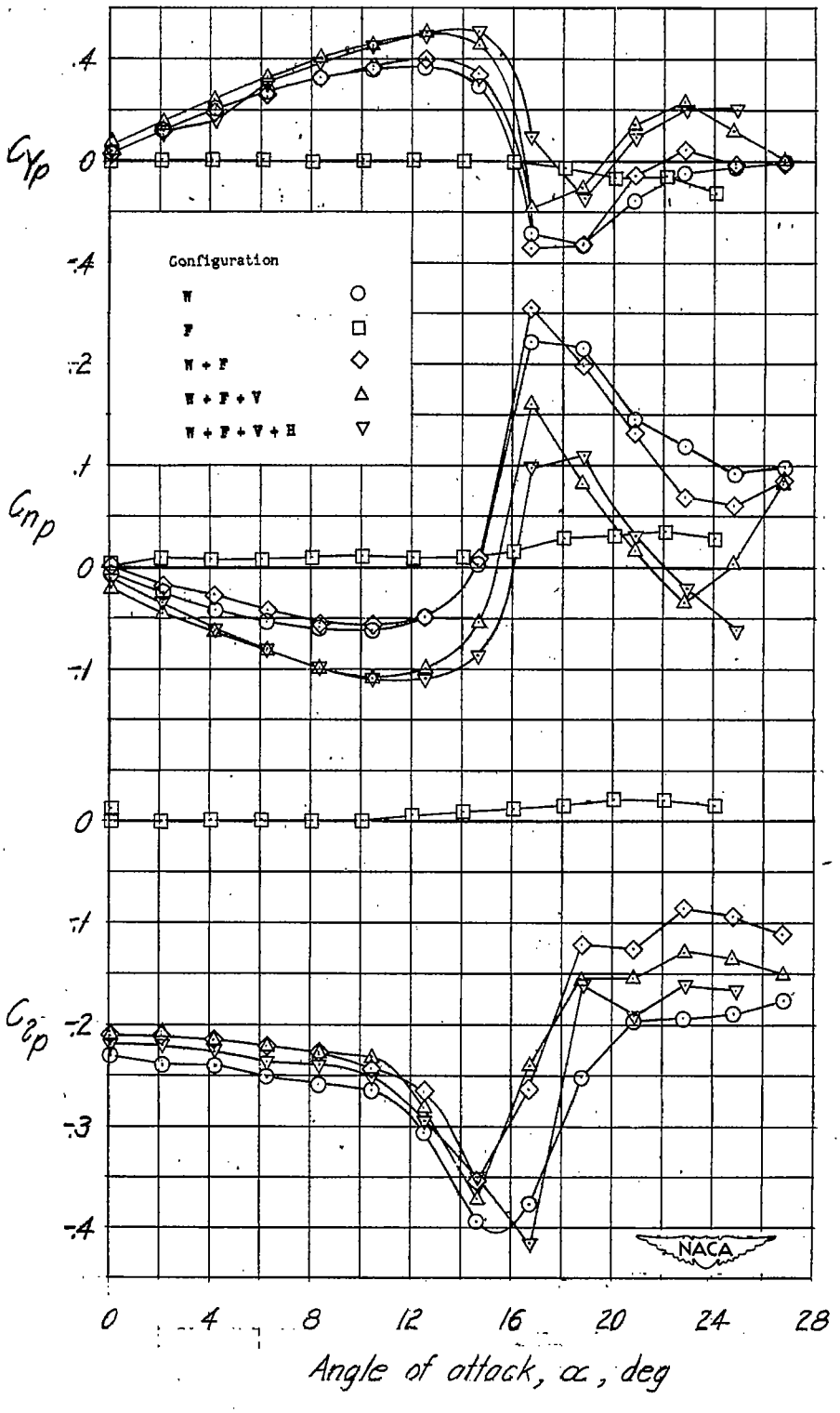

Figure 9.- Variation of C_{l_p}, C_{n_p}, and C_{Y_p} with angle of attack for all model configurations. $\psi = 0^{\circ}$.